

1  
2  
3 **Simultaneous Estimation of Tracer Kinetic Model Parameters Using**  
4 **Analytical and Inverse Approaches with a Hybrid Method**

5  
6 Kokulan Natkunam<sup>1\*</sup>, Yang Hai<sup>1</sup>, Erwin George<sup>1</sup>, Choi-Hong Lai<sup>1</sup>, Li Liu<sup>2</sup>

7 *<sup>1</sup>Department of Mathematical Sciences, University of Greenwich, UK*

8 *<sup>2</sup>Information Centre, Affiliated Hospital of Jiangnan University, 200 Huihe Road, Wuxi 214062,*  
9 *China*

10  
11 *n.kokulan@gre.ac.uk*  
12  
13  
14  
15  
16  
17  
18  
19  
20  
21  
22  
23  
24  
25  
26  
27  
28  
29  
30  
31  
32  
33  
34  
35  
36  
37  
38  
39  
40  
41  
42  
43  
44  
45  
46  
47  
48  
49  
50  
51  
52  
53  
54  
55  
56  
57

For Peer Review Only

58 

---

<sup>1\*</sup> Author correspondence to Kokulan Natkunam , email: [n.kokulan@gre.ac.uk](mailto:n.kokulan@gre.ac.uk)  
59  
60

# Simultaneous Estimation of Tracer Kinetic Model Parameters Using Analytical and Inverse Approaches with a Hybrid Method

## Abstract

The inverse problem approach to Tracer Kinetic Modelling (TKM) using dynamic positron-emission tomography (PET) images is important in identifying the kinetic parameters and then quantifying the tracer concentrations in the region of interest. In parameter estimation, knowledge of good initial approximations to the parameters is essential. The aim of this paper is to extend existing work on an inverse method for tracer kinetics by proposing an improved hybrid method integrated with an analytic solution in a multi-objective formulation of the inverse method. The analytical solution is derived through the use of the Laplace transformation technique. This integrated approach will be compared against other parameter estimation techniques in terms of computational efficiency and accuracy.

Keywords: Tracer kinetic modelling; Inverse problems; Laplace transform; Compartment model; Dynamic PET.

Subject classification code: 62P10, 92C45, 15A29, 80M50, 93C15.

## 1. Introduction

Positron-Emission Tomography (PET) is being used more frequently for treatment of medical conditions and the discovery of drugs [7, 20]. Information relating to radiotracer kinetics, in addition to its spatial distribution, has been discovered through dynamic PET imaging. This information is extremely encouraging for the quantitative interpretation of PET images both in diagnostic and therapeutic contexts.

Tracer Kinetic Modelling (TKM) is the most common methodology for the quantitative interpretation of dynamic PET images. TKM quantifies tracer concentrations in various regions using a set of coupled differential equations (DEs) which describe the tracer behaviour.

TKM requires measurement of both the Plasma Time-Activity Curve (PTAC) and the Tissue Time-Activity Curve (TTAC) to estimate physiological parameters. The PTAC often serves as the input function and the TTAC serves as the output function in TKM.

The DEs contain a set of either (1) kinetic micro parameters describing rate constants associated with inter-compartmental tracer exchange or (2) physiologically meaningful macro parameters that are functions of the underlying micro parameters [3]. The inverse problems approach involves the estimation of these unknown parameters by using experimental data and solutions from the system of DEs. Therefore in the solution process direct problems must be solved. Analytical or numerical methods may be used to solve the direct problems.

The computation begins by assigning an initial guess for the unknown parameters then the direct problem is solved. This is done consecutively until the model solution approaches the experimental data as closely as possible. Knowledge of good initial approximations to the parameters is essential to the estimation of the tracer kinetic parameters. Lack of this information can make the estimation procedure very difficult if not impossible. On the other hand, case studies involving large datasets may be very time consuming. Therefore efficient computation

1  
2  
3 of the inverse problems to determine the kinetic parameters will be able to assist clinicians in  
4 near real time response and judgement of the changes of the tumour. This has profound impact  
5 on effective and accurate treatment of the disease.  
6  
7

8 Specific optimisation methods were studied in an attempt to enhance the effectiveness and  
9 efficiency of parameter estimation of the TKM. Simulated annealing (SA) algorithms were  
10 proposed for the optimisation of the kinetic parameters [21]. These algorithms are based on the  
11 analogy between the state of each molecule and the state of each parameter that affects the energy  
12 function. The FDOPA kinetic model in Parkinson's disease diagnosis was estimated through the particle  
13 swarm optimisation (PSO) method [8].  
14  
15

16 An artificial immune optimisation method was proposed to improve the effectiveness of  
17 parameter estimation [12]. However, it costs much computational time to obtain the optimal  
18 parameters. In a previous related paper [10], we proposed an efficient hybrid parameter  
19 estimation algorithm to fit the compartmental model to the output measurements of  
20 concentration in the region of interest. This hybrid method combines the Quantum-Behaved  
21 Particle Swarm Optimisation (QPSO) and the Levenberg-Marquardt (LM) methods. The QPSO  
22 is a stochastic-based method that helps overcome the difficulty of locating a good initial guess  
23 whilst LM is a gradient-based method that enhances the computational efficiency by speeding up  
24 the process of optimisation. The results presented in that paper demonstrated a speed up in  
25 computational time using the hybrid method in comparison to using the QPSO and PSO  
26 separately, with the same accuracy with regard to experimental data. A similar hybrid approach  
27 was taken in another previous paper [1] which combines QPSO and Gauss-Newton (GN) and  
28 was shown to perform really well in the modelling of cardiac myocyte mechanosensation.  
29  
30  
31  
32  
33

34 In this paper, the hybrid method proposed in [10] is further adapted. An analytic solution of the  
35 direct problem describing the total concentration of the tracer in the region of interest is derived  
36 by means of the Laplace transformation technique for a particular form of the input function  
37 used in this paper. The computational efficiency of the hybrid optimisation method is examined.  
38 In addition, a multi-objective formulation of the inverse problem is used to study the optimal  
39 input and output functions simultaneously.  
40  
41  
42

43 The remaining sections are organised as follows. Section 2 describes the compartmental model  
44 using a system of DEs, the input functions for the tracer in plasma, and a derivation of the  
45 analytical output function. Section 3 focusses on the methodology underlying the inverse  
46 problem formulation including a pseudo code for the hybrid method. In section 4, results are  
47 presented which exhibit the computational accuracy and efficiency of using this hybrid method  
48 in comparison with the QPSO, Particle Swarm Optimisation (PSO) and Differential Evolution  
49 (DE) method [2]. This is then followed by discussions and conclusions.  
50  
51  
52  
53  
54  
55  
56  
57  
58  
59  
60

## 2. Tracer kinetic models

Tracer kinetic models have been used to estimate the cerebral metabolic rate of glucose [14], blood flow, and neuro receptor ligand bindings. Typically, the physiological parameters in tracer kinetic modelling are estimated via PET, which needs the measurements of the tracer time-activity curves in both plasma (PTAC) and tissue (TTAC) in one or more regions of interests (ROIs) of a dynamic image. The fluorodeoxyglucose (FDG) compartmental model is one of the most commonly used tracer kinetic models. Figure 1 shows a two tissue compartmental model for FDG.

[Figure 1 near here]

The tracer enters the plasma via an injection and reaches the tissues of interest. The states of the tracer are extracellular ( $e$ ) and metabolised ( $m$ ). The expressions  $c_e$  and  $c_m$  represent the concentration of the tracer in a “free” (unbound) or “bound” compartment, respectively.

Mathematically, the tracer kinetic model can be expressed as the following system of two ordinary differential equations along with a simple algebraic equation giving the total tracer concentration:

$$\frac{dc_e(t)}{dt} = k_1c_p(t) - (k_2 + k_3)c_e(t) + k_4c_m(t) \quad (1)$$

$$\frac{dc_m(t)}{dt} = k_3c_e(t) - k_4c_m(t) \quad (2)$$

$$c_t(t) = c_m(t) + c_e(t) \quad (3)$$

Here,  $k_1$ ,  $k_2$ ,  $k_3$  and  $k_4$  are model output function parameters that describe the rates of change of FDG between plasma, unbound and bound compartments;  $c_e$  and  $c_m$  represent the concentrations of the tracer in the extracellular state and metabolised state, respectively;  $c_t$  is the output function equal to the sum of the concentrations,  $c_e$  and  $c_m$ , in both compartments; and  $c_p$  is the input function in the plasma.

### 2.1 Input function

The tracer Plasma Time-Activity Curve (PTAC) often serves as the input function of the tracer kinetic models. Measurements of the tracer time-activity curves in both plasma (PTAC) and tissue (TTAC) are used to estimate the physiological parameters in tracer kinetic modelling with PET.

A good estimate of the parameters largely depends on the accuracy of tracer time-activity curves in plasma. The input function is usually given as the sum of a series with exponential terms [6] such as

$$c_p = \sum_{i=1}^n a_i e^{-\lambda_i t}, \quad i = 1, \dots, n \quad (4)$$

where  $a_i$  and  $\lambda_i$  are the parameters of the input function that define the shape of the Plasma Time-Activity Curve.

## 2.2 The analytical output function

A closed form solution for the output function of equations (1)-(3) can be derived by using the Laplace transform and is given below.

Taking the Laplace transform of equations (1) and (2) removes the time dependency and transforms the functions  $c_e(t)$  and  $c_m(t)$  to  $\bar{c}_e(s)$  and  $\bar{c}_m(s)$ . The resulting algebraic equations in terms of the Laplace parameter  $s$  are

$$s\bar{c}_e(s) - c_e(t_0) = k_1\bar{c}_p(s) - (k_2 + k_3)\bar{c}_e(s) + k_4\bar{c}_m(s)$$

$$s\bar{c}_m(s) - c_m(t_0) = k_3\bar{c}_e(s) - k_4\bar{c}_m(s)$$

With initial conditions  $c_e(t_0) = 0$  and  $c_m(t_0) = 0$ , the algebraic system becomes

$$s\bar{c}_e(s) = k_1\bar{c}_p(s) - (k_2 + k_3)\bar{c}_e(s) + k_4\bar{c}_m(s)$$

$$s\bar{c}_m(s) = k_3\bar{c}_e(s) - k_4\bar{c}_m(s).$$

By solving the algebraic equations,  $\bar{c}_e(s)$  and  $\bar{c}_m(s)$  can be obtained. The inverse Laplace transform is then applied to obtain  $c_e(t) = L^{-1}[\bar{c}_e(s)]$  and  $c_m(t) = L^{-1}[\bar{c}_m(s)]$ .

$$c_e(t) = k_1 L^{-1} \left[ \frac{(k_4 + s)}{s^2 + (k_2 + k_3 + k_4)s + k_2 k_4} \right] \otimes c_p(t)$$

$$c_e(t) = k_1 L^{-1} \left[ \frac{k_4 + s}{(s + \alpha)(s + \beta)} \right] \otimes c_p(t)$$

where  $\alpha + \beta = k_2 + k_3 + k_4$  and  $\alpha\beta = k_2 k_4$ .

$$c_e(t) = \frac{k_1}{\beta - \alpha} [(k_4 - \alpha)e^{-\alpha t} + (-k_4 + \beta)e^{-\beta t}] \otimes c_p(t)$$

Similarly for  $c_m(t)$

$$c_m(t) = \frac{k_1 k_3}{\beta - \alpha} [e^{-\alpha t} - e^{-\beta t}] \otimes c_p(t)$$

Given that  $c_m(t) + c_e(t) = c_t(t)$  the following is obtained

$$c_t(t) = \frac{k_1}{\beta - \alpha} [(k_4 + k_3 - \alpha)e^{-\alpha t} + (\beta - k_4 - k_3)e^{-\beta t}] \otimes c_p(t)$$

where  $c_p(t) = \sum_{i=1}^{n=4} a_i e^{-\lambda_i t}$

$$\begin{aligned}
 c_t(t) &= \int_{\tau=0}^t [c_p(\tau)] \left[ \frac{k_1}{\beta - \alpha} [(k_4 + k_3 - \alpha)e^{-\alpha(t-\tau)} + (\beta - k_4 - k_3)e^{-\beta(t-\tau)}] \right] d\tau \\
 c_t(t) &= a_1 \frac{k_1 (k_4 + k_3 - \alpha)}{\beta - \alpha} \left[ \frac{e^{-\lambda_1 t} - e^{-\alpha t}}{\alpha - \lambda_1} \right] + a_2 \frac{k_1 (k_4 + k_3 - \alpha)}{\beta - \alpha} \left[ \frac{e^{-\lambda_2 t} - e^{-\alpha t}}{\alpha - \lambda_2} \right] + a_3 \\
 &\quad \frac{k_1 (k_4 + k_3 - \alpha)}{\beta - \alpha} \left[ \frac{e^{-\lambda_3 t} - e^{-\alpha t}}{\alpha - \lambda_3} \right] + a_4 \frac{k_1 (k_4 + k_3 - \alpha)}{\beta - \alpha} \left[ \frac{e^{-\lambda_4 t} - e^{-\alpha t}}{\alpha - \lambda_4} \right] + a_1 \\
 &\quad \frac{k_1 (\beta - k_4 - k_3)}{\beta - \alpha} \left[ \frac{e^{-\lambda_1 t} - e^{-\beta t}}{\beta - \lambda_1} \right] + a_2 \frac{k_1 (\beta - k_4 - k_3)}{\beta - \alpha} \left[ \frac{e^{-\lambda_2 t} - e^{-\beta t}}{\beta - \lambda_2} \right] + a_3 \\
 &\quad \frac{k_1 (\beta - k_4 - k_3)}{\beta - \alpha} \left[ \frac{e^{-\lambda_3 t} - e^{-\beta t}}{\beta - \lambda_3} \right] + a_4 \frac{k_1 (\beta - k_4 - k_3)}{\beta - \alpha}
 \end{aligned} \tag{5}$$

In the inverse problems approach, the derived analytical formula, equation (5), is used to obtain the optimised parameters in four case studies using two separate optimisation methods: (1) QPSO (2) a hybrid method (a hybrid of QPSO and LM) (3) PSO and (4) DE.

### 3. Inverse problems

The inverse problems [4, 5] approach involves the estimation of unknown parameters that can be determined by using experimental data and solutions from DEs. A commonly used technique in an inverse problem is the Least Squares method in which the sums of the squares of the residuals of the model solution estimates and the experimental data is minimised. This method requires that the estimated solution matches the experimental data as closely as possible over a specified time domain. A multi-objective least squares approach is used for the simultaneous estimation of the tracer kinetic input and output functions.

#### 3.1 The inverse problem formulation for compartment models using simultaneous estimation

In this section, the general formulation of the inverse problem for the tracer kinetic model is given in detail. In order to demonstrate the inverse approach for the tracer kinetic model, the direct problem is first given.

$$\mathbf{C}_t(t) = (c_{t1}(t), c_{t2}(t), \dots, c_{tn}(t))^T$$

$$K = \begin{pmatrix} k_{1,1} & \dots & \dots & k_{1,n} \\ \vdots & & & \vdots \\ k_{n,1} & \dots & \dots & k_{n,n} \end{pmatrix}$$

$$\mathbf{f}(t) = (f_1(t), f_2(t), \dots, f_n(t))^T$$

where  $\mathbf{C}_t(t)$  represents the concentration of the tracer in  $n$  different compartments,  $K$  is a matrix of kinetic parameters and  $\mathbf{f}(t)$  is a non-homogenous term in the ordinary differential equations (ODEs). The compartment model is a system of ODEs involving  $c_t$ , with initial condition  $c_t(t_0)$ , and the input function,  $c_p$ , with initial condition  $c_p(t_0)$ , and it is given as

$$\begin{aligned} \mathbf{C}'_t &= K\mathbf{C}_t + \mathbf{f}(t), \quad \mathbf{C}_t(t_0) = \mathbf{C}_0 \\ c_p &= \sum_{i=1}^n a_i e^{-\lambda_i t}, \quad c_p(t_0) = c_{p0}. \end{aligned}$$

The observation (experimental data) for the output and input functions are distinguished by overbars:

$$\begin{aligned} \overline{\mathbf{C}}_t(t) &= (\overline{c_{t1}}(t), \overline{c_{t2}}(t), \dots, \overline{c_{tn}}(t)) \\ \overline{c}_p(t) &= (\overline{c_{p1}}(t), \overline{c_{p2}}(t), \dots, \overline{c_{pn}}(t)) \end{aligned}$$

The inverse problem formulation involves the objective functions  $J_1(k, a, \lambda)$  and  $J_2(a, \lambda)$ .

$$J_1(k, a, \lambda) = \frac{1}{2} \|c_t(t; k, a, \lambda) - \overline{c}_t(t)\|^2, \quad J_2(a, \lambda) = \frac{1}{2} \|c_p(t; a, \lambda) - \overline{c}_p(t)\|^2$$

where  $k = [k_1, k_2, k_3, k_4]$ ,  $a = [a_1, a_2, a_3, a_4]$ ,  $\lambda = [\lambda_1, \lambda_2, \lambda_3, \lambda_4]$ ,

which are combined into the single multi-objective function

$$w_1 \|c_t(t; k, a, \lambda) - \overline{c}_t(t)\|^2 + w_2 \|c_p(t; a, \lambda) - \overline{c}_p(t)\|^2$$

where  $w_1$  and  $w_2$  are weights.

The aim is to minimise the multi-objective function. Here,  $c_t(t; k)$  can be computed by solving the direct problem as described in Equations (1), (2) and (3) with given values of  $k, a, \lambda$ . Meanwhile  $c_p(t; p)$  can be computed using Equation (4) with the given values of  $a$  and  $\lambda$ .

This inverse problem is ill-posed and has to be regularised in order to stabilise the solution. This optimisation problem can be solved using stochastic algorithms (e.g. PSO, QPSO and genetic algorithms (GAs)) or deterministic algorithms (e.g. gradient descent, Gauss-Newton, Levenberg-Marquardt and the conjugate gradient method).

### 3.2 A Hybrid method for tracer kinetic modelling

The random search associated with stochastic optimisation algorithms leads typically to a slow convergence rate. However, such algorithms have proven reliable in obtaining the global optimum. For relatively fast convergence, deterministic algorithms such as the gradient descent, Gauss Newton, Levenberg-Marquardt and conjugate gradient methods, have demonstrated speed where good model parameter initialisations are given. However, prior information is almost certainly required to obtain good initial parameter values. Through the combination of these two approaches, we have obtained a robust and computationally efficient optimisation method. The proposed new hybrid algorithm is divided into two phases. Firstly, the QPSO investigates the design space thoroughly and identifies the neighbourhood of the global optimum. Once the QPSO process terminates, using a termination condition, the second phase starts by applying the gradient method. This begins with the good estimate from the QPSO and uses the gradient information to accelerate convergence to the global optimum. We shall now outline the QPSO and Levenberg-Marquardt Methods.

### 3.2.1 Quantum-Behaved Particle Swarm Optimisation (QPSO)

The PSO was first developed by Eberhart and Kennedy [9] in 1995. The algorithm uses the behaviour of animals for inspiration, the flocking of birds and the schooling of fish for example.

Finding a solution to an optimisation problem is achieved using a population of particles. Each particle in this population represents a potential solution and an objective fitness function can be used to approximate their position. While the PSO optimisation algorithm shows probabilistic tendencies to global convergence [22], it does not guarantee global convergence in the same way as the QPSO [16,17,18]. Thus QPSO is a global convergence guaranteed [17, 18] search technique which enhances the global search ability of the PSO. We choose QPSO since this global convergence guarantee should lead more reliably to good starting values for the Levenberg-Marquardt algorithm (which might converge very slowly without “good enough” starting values [13]). Unlike PSO, which uses position and velocity vectors, QPSO utilises a wave function to describe the state of each individual particle. The position of these particles and their local focus is updated using

$$x_{i,j}^{n+1} = p_{i,j}^n \pm \alpha |x_{i,j}^n - mbest_j^n| \ln \left( \frac{1}{u_{i,j}^{n+1}} \right) \quad (6)$$

$$p_{i,j}^n = \varphi_{i,j}^n pbest_{i,j}^n + (1 - \varphi_{i,j}^n) gbest_j^n \quad (7)$$

where  $\alpha$  is called the contraction-expansion (CE) coefficient,  $\varphi$  and  $u$  represent uniformly distributed random numbers within  $[0,1]$  and  $gbest$  is the global best position. The mean best position  $mbest$  is defined as the mean value of all particles' best positions

$$mbest_j^n = \sum_{i=1}^M \frac{pbest_i^n}{M}$$

### 3.2.2 Levenberg-Marquardt Methods (LM)

A commonly utilised iterative method for nonlinear least-squares is the Levenberg-Marquardt [11] algorithm, also known as the damped least-squares method, due to its damping parameter  $\lambda$ . To estimate parameters in the compartmental model for tracer kinetic is a nonlinear least-squares problem so the Levenberg-Marquardt method may be used to fit to PET data.

The Levenberg-Marquardt method is based on Gauss-Newton's method which is given below.

$$J^T J \delta p = J^T \bar{f}(p)$$

where  $\bar{f}(p) =$

$$[c_{t1}(t) - \bar{c}_{t1}(t), c_{t2}(t) - \bar{c}_{t2}(t) \cdots, c_{tm}(t) - \bar{c}_{tm}(t), c_{p1}(t) - \bar{c}_{p1}(t), c_{p2}(t) - \bar{c}_{p2}(t) \cdots, c_{pm}(t) - \bar{c}_{pm}(t)]^T$$

The Levenberg-Marquardt method includes an additional damping factor  $\lambda$  given below.

$$[J^T J + \lambda] \delta p = J^T \bar{f}(p) \quad (8)$$



The new set of parameters are updated by solving the above equation for  $\delta p$ . The damping factor is also adjusted for each iteration depending on the current and previous objective function values.

This hybrid algorithm is denoted as QPSO-LM. The proposed algorithm to determine kinetic parameters is displayed through the following pseudo-code:

```

1
2
3
4
5
6
7
8
9
10
11
12
13 While  $e > tolerance$  and ( $iter \leq maxiter$ )
14     Initialise the kinetic parameters  $k_i^n$ ,  $a_i^n$  and  $\lambda_i^n$  for  $i = 1,2,3,4$  in random space for every
15     particle
16     For each particle
17         Solve the ODE models in equation (1)-(4) using numerical or Analytical method
18         Calculate the fitness value
19         If current fitness value  $<$  local fitness value then
20             local position = current position
21             local fitness = current fitness
22         If local fitness  $<$  global fitness value then
23             global position = local position
24             global fitness = local fitness
25     End For
26     For each particle
27         Compute the local focus (attractor)  $p^n$  and then positions  $k_i^{n+1}$ ,  $a_i^{n+1}$  and  $\lambda_i^{n+1}$  for
28          $i = 1,2,3,4$  using equations (7) and (6) respectively
29     End For
30 End While
31 While  $e > tolerance$  and ( $iter \leq maxiter$ )
32     Use parameters obtained in QPSO algorithm as initial values,  $k_i^{n+1}$ ,  $a_i^{n+1}$ , and  $\lambda_i^{n+1}$ 
33     for  $i = 1,2,3,4$ 
34     Solve the ODE models in equation (1)-(4) using numerical or Analytical method
35     Compute Jacobian matrix
36     Calculate the change in parameters using equation (8)
37     Update the new parameters
38 End While

```

#### 4. Numerical experiments

In this section, the inverse problems for both the analytical and numerical case studies are carried out using the experimental data for a single patient from the Nuclear Centre of the Jiangnan University Affiliated Hospital to compare the speed and accuracy of compartmental model fitting.

##### 4.1 Experimental data from PET

Dynamic FDG PET studies were performed at the Nuclear Centre of the University Affiliated Hospital, in Wuxi, China. During this particular set of experiments, five suspected lung cancer patients were enrolled in the study. They were fully informed of the purposes and process of the experiment. None of them was receiving chemotherapy, or other anti-tumour therapy, before scanning. They were also asked not to eat for 4-6 hours before the PET scans and to empty their bladders before the scanning process. During the entire scanning process, they were asked to remain still and silent. The PET scans were obtained by using Siemens Biography True Point 64

PET/CT with 216 mm axial field-of-view (FOV) axial and lateral resolutions 4.2mm, axial resolutions 4.7 mm. dynamic scanning of beds ranged from the lower half of the chest to the upper half of the abdomen area including suspected tumour tissue.

Images were acquired after intravenous injection of 370 MBq  $^{18}\text{F}$ -FDG. The scanning protocol for the dynamic FDG PET studies during the first 30min was:  $8 \times 15\text{s}$  scans,  $6 \times 30\text{s}$  scans,  $5 \times 300\text{s}$  scans according to literature reports [19]. Images were reconstructed using an image iterative method. Image fusion was achieved in coronal, sagittal and transverse view. The ROIs were manually drawn over the PET images to obtain time-activity curves (TACs) on the normal lung tissue, suspected lung tumour tissue and the abdominal aorta region. The abdominal aorta TAC was used as the model input function value of FDG-PET dynamics modelling.

#### 4.2 Results and Discussion

A multi-objective inverse problem is formulated in order to optimise the parameters simultaneously. Computational results are presented for the estimation of output function parameters  $k_i$  and input function parameters  $a_i$  and  $\lambda_i$  for  $i = 1, 2, 3, 4$ . All computational experiments were performed using an Intel core i5 2500, 3.30 GHz with 4GB RAM. Results are obtained and compared between the analytical and numerical methods (the 4th order Runge-Kutta (RK4)). These results are given in Table 1.

For the hybrid method (QPSO-LM), the QPSO algorithm is first run until the norm value for the objective function falls below certain levels which have been given in Table 3. This type of stopping condition is consistent with one of the two convergence criteria described in [15]. Parameters are then used to initialise the LM method so that it starts from the best estimate of the QPSO.

In the hybrid-analytical and numerical method, to test the effect of different initial parameter estimates from the QPSO, we use three different values of the objective function norm as stopping criteria for the QPSO: 15.0, 10.0 and 5.0. The results are given in Table 3 which show that for each of these stopping criteria the parameters converge (with similar overall residual errors), but when 15.0 is used we get greater computational efficiency. When we used stopping criteria values greater than 15.0, the LM method converged more slowly due to starting parameter values which were far from the solutions. Therefore, for our experimental data a stopping condition of 15.0 for the QPSO part of the hybrid method was found to be a good balance between accuracy and efficiency since it meant that we used the expensive QPSO method as much as was needed to get adequate starting parameter estimates for the LM method to converge quickly. The corresponding parameters are given in results columns 1 and 4 of Table 3.

An L2-norm is given for the differences in the input and output functions against the experimental data. This is given as  $(\|r\|_2)_{input}$  for the input function and  $(\|r\|_2)_{output}$  for the output function in Table 1 where the residual  $r = (x_{model} - x_{experimental})$ . A weighted L2-norm is also given for the combined difference of the input and output functions from the experimental data. This is given as  $(\|r\|_2^2)_{total}$ .

1  
2  
3  
4 For all cases, the algorithm is run until the norm value for the output function first falls below  
5 0.63. At this norm value, all of the methods showed good convergence to the data; in addition, it  
6 ensured fair comparisons of the computational times amongst different methods. Algorithms that  
7 achieve errors within this range appear to converge with output and input function results close  
8 to that of the experiments and to each other. Furthermore the final corresponding parameter  
9 values from all simulations are in close agreement.  
10

11  
12 [Figure 2 near here]  
13  
14

15  
16  
17 [Figure 3 near here]  
18  
19

20  
21  
22 Figures 2 and 3 illustrate the accuracy of the model prediction for the output (Figure 2) and input  
23 (Figure 3) functions against the experimental data (red crosses) for the analytical method with  
24 QPSO compared to that of the numerical method with QPSO. The individual methods show  
25 good agreement with the experimental data. Both methods produce very similar results (Figures  
26 2 and 3, Table 1).  
27  
28

29  
30 Similar study was undertaken for the hybrid method and these results can be seen in Figures 4  
31 and 5. Here we also see good agreement between the model output and experimental data for  
32 both the analytical and numerical methods. It also shows that the methods produce similar  
33 results to each other (Figures 4 and 5, Table 1).  
34

35  
36 [Figure 4 near here]  
37  
38

39  
40 [Figure 5 near here]  
41

42 To compare our method with standard evolutionary techniques, similar study was undertaken for  
43 the PSO and DE.  
44

45 PSO results can be seen in Figures 6 and 7. Here we also see good agreement between the  
46 model output and experimental data for both the analytical and numerical methods. It also shows  
47 that the methods produce similar results to each other (Figures 6 and 7, Table 1).  
48  
49

50  
51 [Figure 6 near here]  
52  
53

54  
55 [Figure 7 near here]  
56

57 The results of the DE method can be seen in Figures 8 and 9. Here we also see good agreement  
58 between the model output and experimental data for both the analytical and numerical methods.  
59 It also shows that the methods produce similar results to each other (Figures 8 and 9, Table 1).  
60

[Figure 8 near here]

[Figure 9 near here]

Table 1 shows the obtained values of the parameters and the corresponding  $L_2$ -norm errors obtained using each of the analytical or numerical method for QPSO, the hybrid method, PSO and DE. In all of these case studies, it can be seen that each input and output parameter for the methods are within a small range. Likewise the individual and total error norms are very similar across the four cases.

[Table 1 near here]

[Table 2 near here]

[Table 3 near here]

Table 2 shows the mean computational time taken to run 8 different cases. As can be seen, even though both the analytical and numerical methods provide similar accuracy, the analytical method is much more computationally efficient in comparison with the others. The performance of the hybrid method using the analytical formula outperforms all others with only approximately 2 seconds of run time in comparison with the QPSO, PSO and DE for the analytical method which took about 50, 62 and 20 seconds respectively. Running the LM method with random starting values for the parameters sometimes resulted in relatively quick convergence and sometimes in very slow convergence, indicating a sensitivity to initial conditions. More generally, poor starting values for the LM method could lead to very slow convergence [13] therefore, performing the QPSO method prior to the LM overcomes this issue as well as helps boost the computational efficiency. From these results one can see that the hybrid method is noticeably more computationally efficient than the QPSO, PSO and DE alone. Additionally, we see a noticeable computational speed up when using the analytical method. Overall, the hybrid-analytical method outperforms the rest.

## 5. Conclusion and future work

In this paper, we investigated the fast and efficient improved simultaneous estimation of tracer kinetic models using an analytical formula for the direct problem and a hybrid method which

combines the stochastic optimisation method, QPSO, and the gradient based optimisation method, LM, for identifying parameters in tracer kinetic modelling.

The model predicted results show good agreement with experimental data from the Nuclear Centre of the University Affiliated Hospital, in Wuxi, China. The performance of the hybrid method using the analytical solution for the total tracer concentration was tested and compared with QPSO, PSO and DE to show that the computational time for the hybrid method is much less expensive. This enables the method to be used for fitting any PET data accurately and robustly in fewer than 3 seconds. In addition, this method automatically finds an initial approximation that aids convergence of the scheme and which overcomes the difficulty of finding a suitable initial approximation for the tracer kinetic parameters. This hybrid approach demonstrated substantial reduction in computational times. One potential clinical impact of this research is that the result tool provides rapid confirmation in real time of any presence or changes of a tumor resulting to early treatment plan.

Future research includes implementing time domain parallel computing techniques to solve for the parameters in nonlinear compartment TKMs to further improve the computational speed up and the development of the computational tool into clinical applications as discussed above.

#### Acknowledgments

The work of Kokulan is supported by the REF funding of the University of Greenwich. The work of Hai was supported by a PhD bursary of the University of Greenwich. The work of Liu was supported by the National Natural Science Foundation of China (No.61300150), and the Wuxi Municipal Commission of Health and Family Planning (No.YGZXZ1302).

#### References

- [1] S. Arif, N. Kokulan, B. Buyandelger, C.-H. Lai and R. Knoll, *Inverse problem approach to identify the internal force of a mechanosensation process in a cardiac myocyte*, Inf Med Unlocked, 6 (2017), pp. 36-42.
- [2] U.K.Chakraborty, *Advances in differential evolution*, Springer,2008.
- [3] J. Dutt and R. M. Leahy, Q. Li, *Non-local means denoising of dynamic PET images*, PloS one. 8 (2013), pp. e81390.
- [4] W. Fan, X. Jiang, and H. Qi, *Parameter estimation for the generalized fractional element network Zener model based on the Bayesian method*, Physica A, 427 (2015), pp.40-49.
- [5] W. Fan, F. Liu, X. Jiang and I. Turner, *Some novel numerical techniques for an inverse problem of the multi-term time fractional partial differential equation*, J. Comput. Appl. Math, 336 (2018), pp.114-126.
- [6] D. Feng, S.-C. Huang and X. Wang, *Models for computer simulation studies of input functions for tracer kinetic modeling with positron emission tomography*, Int. J. Biomed. Comput. 32 (1993), pp. 95-110.
- [7] P. He, S. J. Haswell, N. Pamme and S. J. Archibald, *Advances in processes for PET radiotracer synthesis: Separation of [18F] fluoride from enriched [18O] water*, Appl. Radiat. Isot. 91 (2014), pp. 64-70.

- 1  
2  
3 [8] C. K. Huang, W. C. Wang, K. Y. Tzen, W. L. Lin and C.Y. Chou, *FDOPA Kinetics Analysis in Pet*  
4 *Images for Parkinson's Disease Diagnosis by Use of Particle Swarm Optimization*, 9th IEEE  
5 International Symposium on Biomedical Imaging, Barcelona, Spain, 2012, pp. 586-589.  
6 [9] J. Kennedy and R. Eberhart, *Particle Swarm Optimization*, IEEE Int'l. Conf. on Neural Networks,  
7 Perth, Australia, 1995, pp. 1942-1948  
8 [10] N. Kokulan, Y. Hai, E. George, C. H. Lai and L. Liu, *An inverse method for tracer kinetic*  
9 *modelling with positron emission tomography (PET) using hybrid method*, Smart Cities  
10 Conference (ISC2), IEEE International, Trento, Italy, 2016, pp. 1-6.  
11 [11] K. Levenberg, *A method for the solution of certain non-linear problems in least squares*, Q. Appl.  
12 Math. 2 (1944), pp. 164-168.  
13 [12] L. Liu, H. Ding, H. B. Huang, *Improved simultaneous estimation of tracer kinetic models with*  
14 *artificial immune network based optimization method*, Appl. Radiat. Isot. 107 (2016), pp. 71-76.  
15 [13] J.Nocedal and S.J.Wright, *Numerical optimisation*, Springer Science, Berlin, 1999.  
16 [14] M.E. Phelps, S.C. Huang, E.J. Hoffman, C. Selin, L. Sokoloff and D.E. Kuhl, *To- mographic*  
17 *measurement of local cerebral glucose metabolic rate in humans with (F-18)2-fluoro-2-deoxy-D-*  
18 *glucose validation of method*, Ann. Neurol. 6 (1979), pp. 371-388.  
19 [15] Plevris and M.Papadrakakis, *A Hybrid Particle Swarm-Gradient Algorithm for Global Structural*  
20 *Optimization*, Comput. Aided. Civ. Inf. 26 (2011), pp. 48-68.  
21 [16] J. Sun, C.-H. Lai and X.-J. Wu, *Particle swarm optimisation classical and quantum perspectives*,  
22 CRC Press, Boca Raton, FL 2011.  
23 [17] J. Sun, W. Fang, X. J. Wu, V. Palade and W. Xu, *Quantum-behaved particle swarm optimization:*  
24 *analysis of individual particle behavior and parameter selection*, Evol. Comput. 20 (2012), pp.349-  
25 393.  
26 [18] J. Sun, X. Wu, V. Palade, W. Fang, C.-H. Lai, and W. Xu, *Convergence analysis and*  
27 *improvements of quantum-behaved particle swarm optimization*, J.Inf.Sci. 193 (2012), pp. 81-103.  
28 [19] T.Torizuka, S.Nobezawa and S.Momiki, *Short dynamic FDG-PET imaging protocol for patients*  
29 *with lung cancer*, Eur. J. Nucl. Med. Mol, 27 (2000), pp.1538-1542.  
30 [20] K.Varnas, A.Varrone and L.Farde, *Modeling of PET data in CNS drug discovery and*  
31 *development*, J. Pharmacokinet. Pharmacodyn. 40 (2013), pp. 267-279.  
32 [21] K.P.Wong, S.R Meikle, D. G Feng and M.J Fulham, *Estimation of input function and kinetic*  
33 *parameters using simulated annealing application in a flow model*, IEEE Transactions on Nuclear  
34 Science, 2002, pp. 707-713.  
35 [22] G. Xu and G. Yu, *Reprint of: On convergence analysis of particle swarm optimization algorithm*,  
36 J. Comp. Appl. Math. 340 (2018), pp. 709-717.  
37  
38  
39  
40  
41  
42  
43  
44  
45  
46  
47  
48  
49  
50  
51  
52  
53  
54  
55  
56  
57  
58  
59  
60

	Parameters	Analytical				Numerical			
		Hybrid Method	QPSO	PSO	DE	Hybrid	QPSO	PSO	DE
Output	K1	0.756	0.749	0.746	0.705	0.729	0.736	0.734	0.627
	K2	5.501	5.675	5.668	5.626	5.811	5.748	5.738	5.398259
	K3	0.830	0.862	0.853	0.955	0.971	0.963	0.949	0.970687
	K4	0.026	0.025	0.022	0.028	0.0206	0.0211	0.014	0.016346
Input	$a_1$	-540.254	-539.508	-538.824	-538.711	-540.322	-539.466	-539.671	-540.905
	$a_2$	480.005	479.259	479.092	474.786	479.939	480.118	479.523	473.1528
	$a_3$	56.440	56.441	56.029	60.276	56.5016	55.540	56.304	63.68118
	$a_4$	3.820	3.826	3.816	3.855	3.886	3.797	3.845	3.867833
	$\lambda_1$	11.088	11.069	11.024	10.541	11.442	11.834	11.794	11.16894
	$\lambda_2$	13.436	13.400	13.317	12.646	14.152	15.000	15.168	14.009
	$\lambda_3$	3.412	03.400	3.370	3.514	3.451	3.400	3.360	3.647512
	$\lambda_4$	0.0336	0.034	0.035	0.0352	0.035	0.0351	0.039	0.035935
$L_2$ -Norm	$(\ r\ _2)_{total}$	1.154	1.073	1.165	1.192	1.111	1.109	1.148	1.092
	$(\ r\ _2)_{output}$	0.621	0.608	0.602	0.6150	0.584	0.604	0.5950	0.5981
	$(\ r\ _2)_{input}$	1.881	1.890	1.918	1.9638	1.881	1.803	1.8906	1.772

**Table 1:** Comparison of parameter estimation and errors for hybrid, QPSO, PSO and DE using analytical and numerical method

	Method	Computational time (s)
Analytical	Hybrid Method	2.28
	QPSO	50.90
	PSO	62.51
	DE	19.42
Numerical	Hybrid Method	9.20
	QPSO	114.00
	PSO	132.39
	DE	56.13

**Table 2:** Computational time

	Parameters	Analytical-Hybrid Stopping Criteria of QPSO			Numerical-Hybrid Stopping Criteria of QPSO		
		Epsilon=15	Epsilon=10	Epsilon=5	Epsilon=15	Epsilon =10	Epsilon =5
Output	K1	0.756	0.803	0.757	0.729	0.736	0.702
	K2	5.501	5.672	5.684	5.811	5.814	5.846
	K3	0.830	0.785	0.842	0.971	0.954	1.032
	K4	0.026	0.0246	0.024	0.0206	0.020	0.022
Input	$a_1$	-540.254	-539.540	-538.995	-540.322	-539.849	-539.668
	$a_2$	480.005	480.541	479.003	479.939	479.504	479.466
	$a_3$	56.440	55.220	56.088	56.5016	56.455	56.359
	$a_4$	3.820	3.813	3.891	3.886	3.893	3.871
	$\lambda_1$	11.088	11.120	11.050	11.442	11.723	11.652
	$\lambda_2$	13.436	13.437	13.335	14.152	14.780	14.615
	$\lambda_3$	3.412	3.380	3.422	3.451	3.467	3.455
	$\lambda_4$	0.0336	0.0334	0.03527	0.035	0.0354	0.0348
$L_2$ -Norm	$(\ r\ _2)_{total}$	1.154	1.1629	1.1554	1.111	1.0921	1.0902
	$(\ r\ _2)_{output}$	0.621	0.6188	0.6028	0.584	0.5888	0.5679
	$(\ r\ _2)_{input}$	1.881	1.9011	1.8979	1.881	1.779	1.791

**Table 3:** Comparison of the effect of different stopping conditions on the parameter estimations and errors of the hybrid method



1  
2  
3  
4  
5  
6  
7  
8  
9  
10  
11  
12  
13  
14  
15  
16  
17  
18  
19  
20  
21  
22  
23  
24  
25  
26  
27  
28  
29  
30  
31  
32  
33  
34  
35  
36  
37  
38  
39  
40  
41  
42  
43  
44  
45  
46  
47  
48  
49  
50  
51  
52  
53  
54  
55  
56  
57  
58  
59  
60

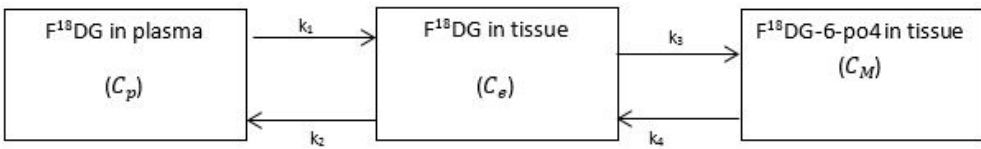


Figure 1: Two tissue compartmental model

160x23mm (96 x 96 DPI)

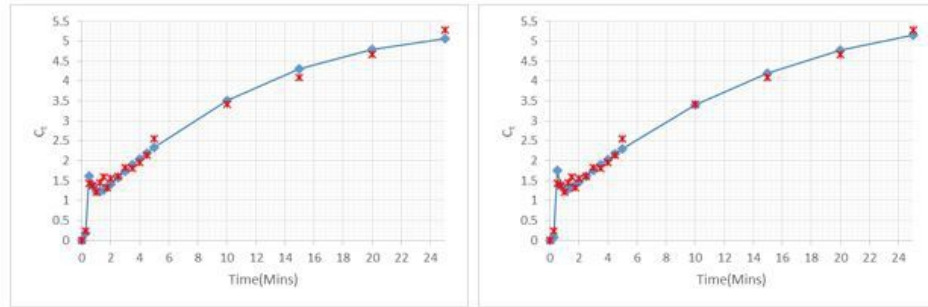


Figure 2: The concentration of the output function ( $C_t$ ) predicted by the model (solid line) is compared against the experimental data (starred). For the model prediction an analytical method (left) and a numerical method (right) are used and obtained using the QPSO method.

55x17mm (300 x 300 DPI)

1  
2  
3  
4  
5  
6  
7  
8  
9  
10  
11  
12  
13  
14  
15  
16  
17  
18  
19  
20  
21  
22  
23  
24  
25  
26  
27  
28  
29  
30  
31  
32  
33  
34  
35  
36  
37  
38  
39  
40  
41  
42  
43  
44  
45  
46  
47  
48  
49  
50  
51  
52  
53  
54  
55  
56  
57  
58  
59  
60

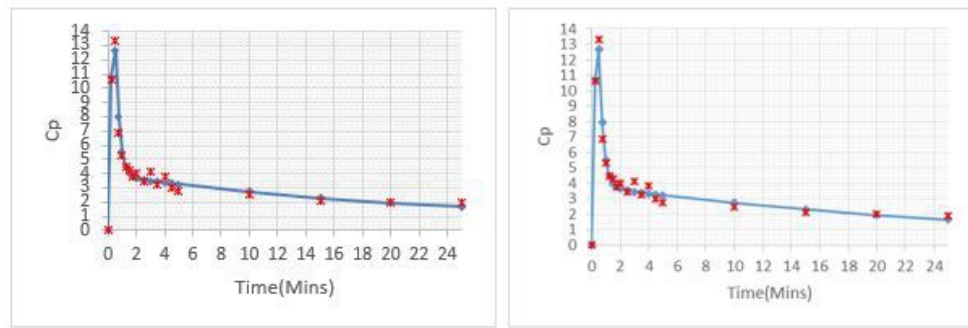


Figure 3: The concentration of the Input function ( $C_p$ ) predicted by the model (solid line) is compared against the experimental data (starred). For the model prediction an analytical method (left) and a numerical method (right) are used and obtained using the QPSO method.

52x17mm (300 x 300 DPI)

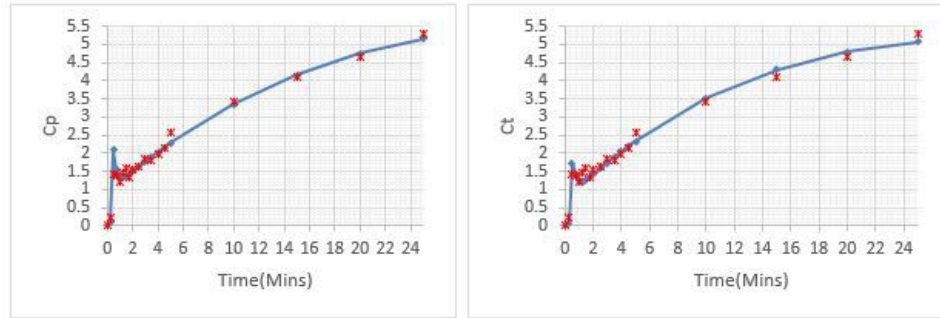


Figure 4: The concentration of the output function ( $C_p$ ) predicted by the model (solid line) is compared against the experimental data (starred). For the model prediction an analytical method (left) and a numerical method (right) are used and obtained using the hybrid method.

54x18mm (300 x 300 DPI)

1  
2  
3  
4  
5  
6  
7  
8  
9  
10  
11  
12  
13  
14  
15  
16  
17  
18  
19  
20  
21  
22  
23  
24  
25  
26  
27  
28  
29  
30  
31  
32  
33  
34  
35  
36  
37  
38  
39  
40  
41  
42  
43  
44  
45  
46  
47  
48  
49  
50  
51  
52  
53  
54  
55  
56  
57  
58  
59  
60

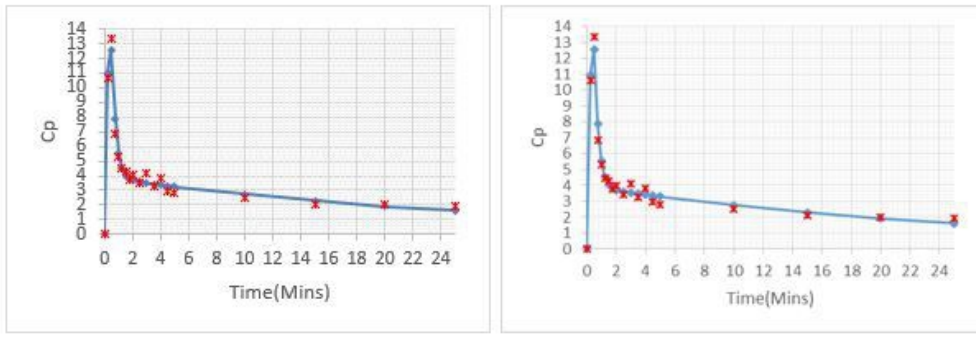


Figure 5: The concentration of the Input put function ( $C_p$ ) predicted by the model (solid line) is compared against the experimental data (starred). For the model prediction an analytical method (left) and a numerical method (right) are used and obtained using the hybrid method.

51x18mm (300 x 300 DPI)

1  
2  
3  
4  
5  
6  
7  
8  
9  
10  
11  
12  
13  
14  
15  
16  
17  
18  
19  
20  
21  
22  
23  
24  
25  
26  
27  
28  
29  
30  
31  
32  
33  
34  
35  
36  
37  
38  
39  
40  
41  
42  
43  
44  
45  
46  
47  
48  
49  
50  
51  
52  
53  
54  
55  
56  
57  
58  
59  
60

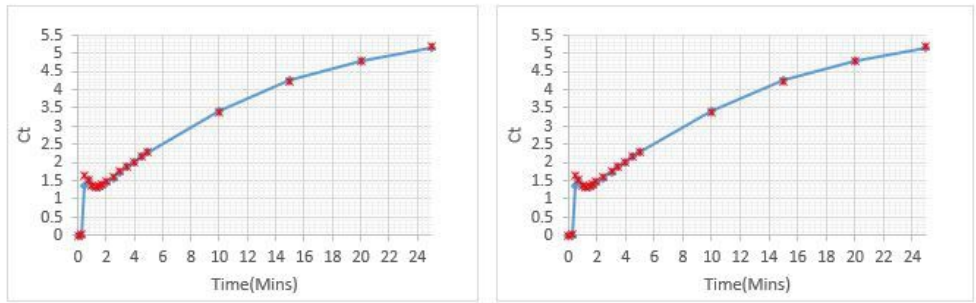


Figure 6: The concentration of the Input put function ( $C_t$ ) predicted by the model (solid line) is compared against the experimental data (starred). For the model prediction an analytical method (left) and a numerical method (right) are used and obtained using the PSO.

57x18mm (300 x 300 DPI)

1  
2  
3  
4  
5  
6  
7  
8  
9  
10  
11  
12  
13  
14  
15  
16  
17  
18  
19  
20  
21  
22  
23  
24  
25  
26  
27  
28  
29  
30  
31  
32  
33  
34  
35  
36  
37  
38  
39  
40  
41  
42  
43  
44  
45  
46  
47  
48  
49  
50  
51  
52  
53  
54  
55  
56  
57  
58  
59  
60

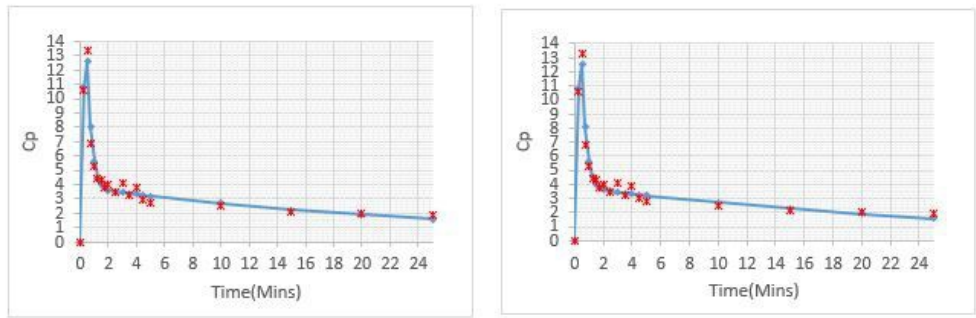


Figure 7: The concentration of the Input put function ( $C_p$ ) predicted by the model (solid line) is compared against the experimental data (starred). For the model prediction an analytical method (left) and a numerical method (right) are used and obtained using the PSO.

55x18mm (300 x 300 DPI)

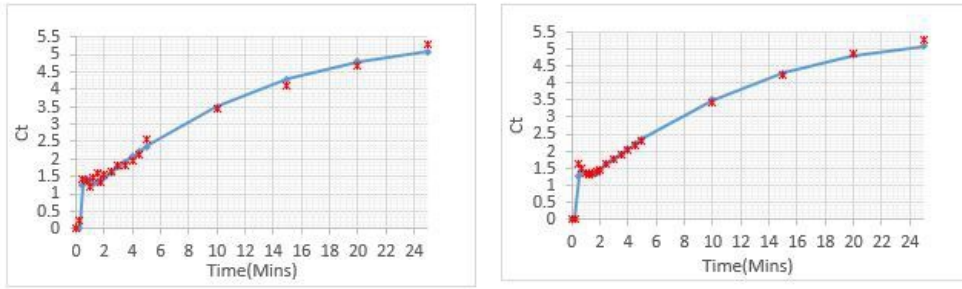


Figure 8: The concentration of the Input put function ( $C_t$ ) predicted by the model (solid line) is compared against the experimental data (starred). For the model prediction an analytical method (left) and a numerical method (right) are used and obtained using the DE.

55x17mm (300 x 300 DPI)



1  
2  
3  
4  
5  
6  
7  
8  
9  
10  
11  
12  
13  
14  
15  
16  
17  
18  
19  
20  
21  
22  
23  
24  
25  
26  
27  
28  
29  
30  
31  
32  
33  
34  
35  
36  
37  
38  
39  
40  
41  
42  
43  
44  
45  
46  
47  
48  
49  
50  
51  
52  
53  
54  
55  
56  
57  
58  
59  
60

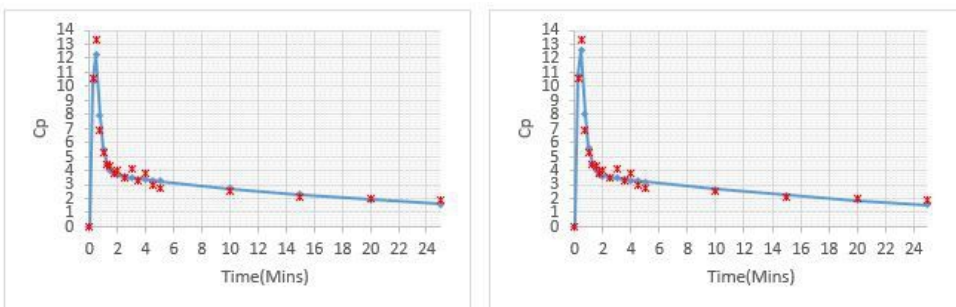


Figure 9: The concentration of the Input put function ( $C_p$ ) predicted by the model (solid line) is compared against the experimental data (starred). For the model prediction an analytical method (left) and a numerical method (right) are used and obtained using the DE.

57x18mm (300 x 300 DPI)

1  
2  
3 **Figure 1:** Two tissue compartmental model  
4

5 **Figure 2:** The concentration of the output function ( $C_t$ ) predicted by the model (solid line) is  
6 compared against the experimental data (starred). For the model prediction an analytical method  
7 (left) and a numerical method (right) are used and obtained using the QPSO method.  
8

9  
10 **Figure 3:** The concentration of the Input function ( $C_p$ ) predicted by the model (solid line) is  
11 compared against the experimental data (starred). For the model prediction an analytical method  
12 (left) and a numerical method (right) are used and obtained using the QPSO method.  
13

14 **Figure 4:** The concentration of the output function ( $C_t$ ) predicted by the model (solid line) is  
15 compared against the experimental data (starred). For the model prediction an analytical method  
16 (left) and a numerical method (right) are used and obtained using the hybrid method.  
17

18  
19  
20 **Figure 5:** The concentration of the Input put function ( $C_p$ ) predicted by the model (solid line) is  
21 compared against the experimental data (starred). For the model prediction an analytical method  
22 (left) and a numerical method (right) are used and obtained using the hybrid method.  
23

24 **Figure 6:** The concentration of the Input put function ( $C_t$ ) predicted by the model (solid line) is  
25 compared against the experimental data (starred). For the model prediction an analytical method  
26 (left) and a numerical method (right) are used and obtained using the PSO.  
27

28  
29 **Figure 7:** The concentration of the Input put function ( $C_p$ ) predicted by the model (solid line) is  
30 compared against the experimental data (starred). For the model prediction an analytical method  
31 (left) and a numerical method (right) are used and obtained using the PSO.  
32

33 **Figure 8:** The concentration of the Input put function ( $C_t$ ) predicted by the model (solid line) is  
34 compared against the experimental data (starred). For the model prediction an analytical method  
35 (left) and a numerical method (right) are used and obtained using the DE.  
36

37  
38 **Figure 9:** The concentration of the Input put function ( $C_p$ ) predicted by the model (solid line) is  
39 compared against the experimental data (starred). For the model prediction an analytical method  
40 (left) and a numerical method (right) are used and obtained using the DE.  
41  
42  
43  
44  
45  
46  
47  
48  
49  
50  
51  
52  
53  
54  
55  
56  
57  
58  
59  
60